NASA Technical Memorandum 101471
AIAA-89-0070

Behavior in Normal and Reduced Gravity of an Enclosed Liquid/Gas System With Nonuniform Heating From Above

H.D. Ross
Lewis Research Center
Cleveland, Ohio

D.N. Schiller
University of California at Irvine
Irvine, California

P. Disimile
University of Cincinnati
Cincinnati, Ohio

and

W.A. Sirignano
University of California at Irvine
Irvine, California

Prepared for the
27th Aerospace Sciences Meeting
sponsored by the American Institute of Aeronautics and Astronautics
Reno, Nevada, January 9–12, 1989

Behavior in Normal and Reduced Gravity of An Enclosed Liquid/Gas System with Nonuniform Heating From Above

H. D. Ross*, D. N. Schiller†, P. Disimile‡, and W. A. Sirignano§

Abstract

The temperature and velocity fields have been investigated for a single-phase gas system and a two-layer gas-and-liquid system enclosed in a circular cylinder being heated suddenly and nonuniformly from above. The transient response of the gas, liquid, and container walls was modelled numerically in normal and reduced gravity (10^{-5}g). Verification of the model was accomplished via flow visualization experiments in 10 cm high by 10 cm diameter plexiglass cylinders.

Introduction

The ignition and flame spread characteristics of liquid fuel pools are subjects of considerable scientific interest and are very relevant to fire safety applications in such areas as aircraft crashes and petroleum spills. In many accident situations, including those which can occur in space, a flammable liquid is spilled in the vicinity of an ignition source. Another prototypical hazard situation might be the rupture of a fuel tank when hot engine parts or exhaust gases may appear in close proximity of liquid fuel. Pool fires are complicated by multiple energy and mass transport processes, phase change, and chemical reaction. It is believed that reduced gravity will remove or isolate some of these complications. However, the scientific literature is devoid of experimental study of these characteristics under conditions of reduced gravity. This paper is primarily concerned with the effects of gravity on the convective flow and temperature fields which occur prior to the ignition of a pool of liquid fuel.

In the presence of an ignition source, liquid motion will be driven by both surface-tension gradients and by liquid buoyancy. These driving forces generally support in concert surface fluid motion away from the source. Therefore this motion tends to delay ignition as heat from the source is convected away rather than concentrated. On the other hand, the motion supports flame spread as the convection assists the preheating process ahead of the flame. The role of gravity varies depending on the relative strengths of buoyancy versus surface tension in driving the convection. If buoyancy contributes significantly, then a reduction in gravity will lead to more rapid ignition but slower flame spread. If the surface-tension gradients dominate, as generally thought, one might envision a longer ignition delay but a more rapid flame spread in reduced gravity.

Theoretical studies in the literature[1,2,3] often assume that surface tension is the principal mechanism for motion of the liquid fuel ahead of the flame front for small laboratory scale experiments. However, in an attempt to isolate the effects of the two forces, Murad et al.[4] added a surfactant to a fuel which eliminated the temperature dependence of surface tension in the temperature range of interest. The effect of the surfactant was to reduce the ignition delay time, but to a much lesser extent than described above for the viscosity-enhanced fuel. They concluded that both forces, surface tension and buoyancy, were important to the ignition problem. The authors did not isolate the effect of buoyancy in their experiments; experiments in reduced gravity allow such isolation to be accomplished. Recent theoretical studies[5,6] indicate that surface tension dominates only below a Grashof number of 10^4.

The importance of gas phase processes has not been treated quantitatively until recently[1,5,6]. While providing fresh oxidizer to a spreading flame, gas phase buoyancy in normal gravity was predicted to be very strong in the vicinity of the flame front. When the Grashof number was set equal to zero, the flame position shifted much closer to the liquid surface. This flame position shift is opposite that observed for solid surface burning in microgravity experiments[7]. In the solid surface case, the reduction in gravity moved the flame further from the solid surface presumably due to an inability of oxidizer to diffuse inwards in the absence of buoyancy. In the liquid pool burning case, however, liquid motion due to surface tension provides a possible convective mechanism for oxidizer to be entrained and brought close to the surface. If the flame resides closer to the surface, gas conduction, flame radiation, and the vaporization process differ from the case of normal gravity. Ignition delays will differ as well.

*Research Engineer, NASA-Lewis Research Center.

†Research Assistant, University of California at Irvine, Irvine, CA 92664; member AIAA.

‡Assistant Professor, University of Cincinnati, Cincinnati, OH 45221.

§Professor of Mechanical Engineering, University of California at Irvine, Irvine, CA 92664; AIAA Fellow.

Problem Description

As a first step in a combined computational and experimental study, the temperature and velocity fields were investigated for an enclosed circular cylinder heated suddenly and nonuniformly from above. The axisymmetric geometry of the problem is shown in Figure 1. One

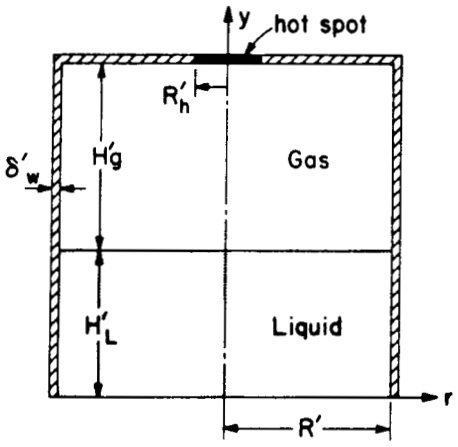

Figure 1: Geometry of the problem.

or two fluids (gas or gas-liquid) were contained in the cylinder. Initially the entire system was quiescent and at constant temperature. In the center of the top surface, a spot heater was surrounded by a water-cooled jacket. This spot heater with a known radial temperature profile was then suddenly energized. Once heating began, the response of the system in terms of velocity and temperature was determined numerically. As a verification of the model, the flow patterns were determined experimentally.

The first series of tests involved a container filled only with a single gas phase. The second series of tests involved liquid and gas phases, but with the liquid being non-evaporative. The third series of tests involved two phases with the liquid being evaporative. The fourth series of tests will involve ignition and flame spread of the evaporated fuel. However, in this paper only the first two cases are discussed; also the reduced gravity tests are restricted to the single phase problem.

Numerical Model Description

The finite-difference procedure applied to the governing equations in the gas and liquid phases utilizes the SIMPLE algorithm[8] with the SIMPLEC modification[9]. The numerical model uses primitive variables (u, v, p, h), a staggered mesh[8], and variable thermophysical properties (density, viscosity, etc.) in both phases. Variable density is important in the gas phase because during preignition heating, high temperature gradients are expected near the ignition source (i.e., the heater). In such a situation, the use of a constant density approach along with the Boussinesq approximation may produce very serious quantitative errors in the analysis of the phenomenon. The incorporation of variable thermophysical properties in the liquid phase is also very important since the viscosity and volume expansion coefficient of many liquids vary considerably with temperature.

The effects of surface tension, evaporation, radiation, and wall thermal inertia are incorporated into the computational code. All surfaces are assumed to have an emissivity of 1.0. The calculation of the radiative heat transfer between elementary rings of the enclosure and liquid surface has been described previously by Abramzon, Edwards, and Sirignano[6]. The program also accounts for the total pressure variations in the gas phase. This option is very important for the enclosed container simulations because the total gas pressure is continuously increasing during the heating and vaporization processes. The code also allows for local refining of the finite-difference grid at regions where the field gradients are large and better resolution of the problem is needed.

The following variables are allowed to be changed parametrically:

- Liquid fill level.
- Container dimensions, including wall thickness.
- Thermal driving potential (heater temperature and size).
- Fluid properties.
- Gravity level.

The gas and liquid phase solutions are time-split in that the solution at time t represents the gas phase at time t and the liquid phase at time $t + \frac{1}{2}\Delta t$ (where Δt is the time step). At the liquid-vapor interface, values of liquid temperature and velocity are used for the gas phase solution while values of gradients of gas temperatures and velocities are used for the liquid phase solution. Because the prediction of the time-dependent liquid-vapor interfacial shape is beyond the state of the art, the model presently considers only a flat liquid-vapor interface. The sequential calculation procedure for each time step is as follows:

- Determine wall boundary temperatures using explicit scheme:
  1. Calculate total heat fluxes (radiative + conductive) to the walls in the gas phase based on temperatures at time t.
  2. Calculate conductive heat fluxes to the walls in the liquid phase based on temperatures at time t.
  3. Use explicit scheme to calculate wall temperatures based on above heat flux data. Newton's law of cooling is used as a boundary condition at the outside wall to take into account natural convection to the environment.
- Determine gas phase solution at time $t + \Delta t$:

1. Calculate gas phase properties at beginning of time step. Only values of c_p are updated during the internal iteration cycle. This helps stabilize the solution. Values of c_p are updated in order to update values of enthalpy.
2. Perform internal iteration loop for gas phase (SIMPLE algorithm). Boundary values of wall temperatures (from explicit solution) and liquid temperatures and velocities (from time $t + \frac{1}{2}\Delta t$) are used.

- Determine liquid phase solution at time $t + \frac{3}{2}\Delta t$:
  1. Calculate liquid phase properties at beginning of time step. Only values of c_p are updated during the internal iteration cycle.
  2. Perform internal iteration loop for liquid phase (SIMPLE algorithm). Boundary values of wall temperatures (from explicit solution) and gradients of gas temperatures and velocities (from time $t + \Delta t$) are used (e.g., heat and stress balances at interface). The bottom of the liquid phase is assumed to be isothermal at the reference temperature.

As previously mentioned, the resulting solution for time $t + \Delta t$ actually represents the gas phase at time $t + \Delta t$ and the liquid phase at time $t + \frac{3}{2}\Delta t$. The calculation procedure for the single-phase simulation is similar to the above except that a relatively thick, isothermal wall is used at the bottom of the gas phase.

The calculations were performed with a 22 x 22 mesh in each phase. Since 2 boundary nodes are used in each direction, there are 20 x 20 internal cells in this mesh. Denser meshes were employed to test grid sensitivity with no significant differences in the results. The time step was typically about 0.05 s and required about 8 s of CPU time on a VAX-11/780 computer for the two-phase calculations, and about 4 s of CPU time for the single-phase calculations.

Experimental Apparatus Description

Figure 2 displays schematically the experimental setup used to determine the flow patterns. The entire apparatus was constructed inside a "drop rig" used in low-gravity drop tower tests. The test cell had a 0.4 cm wall thickness and a 10 cm height and diameter. In the center of the top surface, a 2.5 cm copper water-cooled jacket was employed to prevent the top surface from melting and to concentrate the heating from above. The heater itself was a thin nichrome wire wrapped in ceramic cement. A Type K thermocouple was flush mounted at the center of the exposed surface of the heater. Both the axisymmetry and the radial temperature distribution of the heater were checked via the use of an infrared radiometer. A series of heaters with a different wiring pattern were discarded

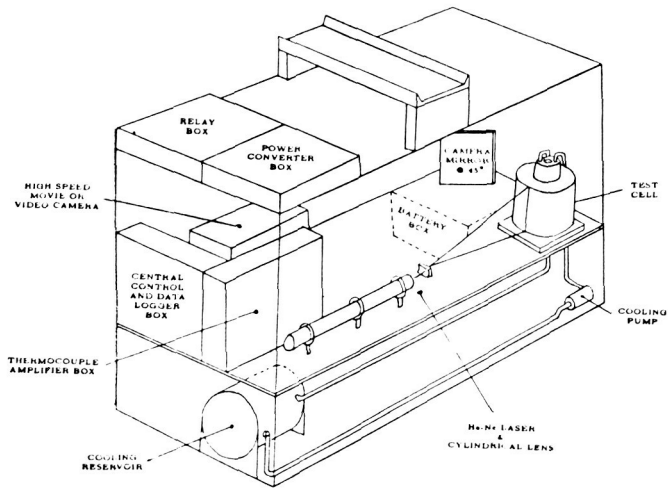

Figure 2: Schematic view of the test cell arrangement.

because they had an asymmetric temperature distribution. Figure 3 displays typical radiometric photographs of the heaters. The radial temperature distribution used in the simulations was deduced from these radiometric measurements.

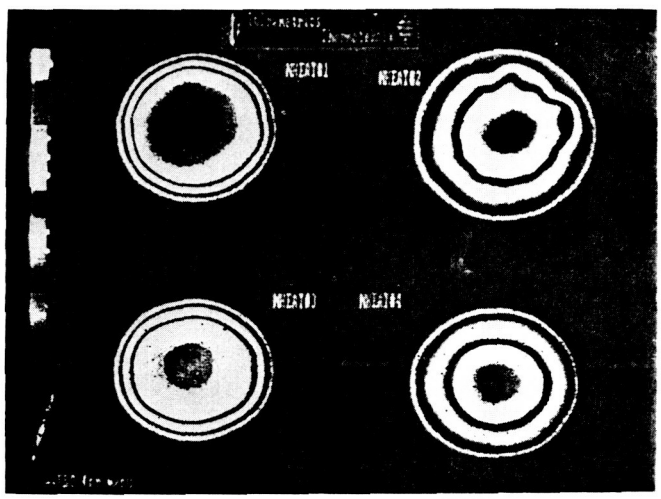

Figure 3: Radiometric photographs of four heaters. Heaters #1 and #2 were rejected.

The flow was visualized via tracers (either smoke, aerosol droplets, or aluminum oxide particles) illuminated in a single plane by a light sheet. The flow patterns were recorded on video tape and/or motion picture film. The light sheet was created by use of a 5 mW Helium-Neon laser passing through a cylindrical lens. The laser light was then reflected back by a mirror (not shown on Figure 2) to double the illumination. No effect of the laser

light absorption was observed. Some tests were run with two lasers operating from different angles relative to the camera, allowing a check of the axisymmetry assumption. Except as noted below, the system was found to behave in the expected, axisymmetric configuration.

In the single-phase tests, a cigarette smoke tracer was blown into the cell prior to heating and its motion allowed to settle for 5 minutes. Two kinds of heater scenarios were employed. In most cases, the heater was mounted in place when it was energized at a preset voltage and current. Within 60 seconds, the heater reached its steady state temperature. In some cases the heater was brought up to temperature away from the rig, then placed quickly into position. The latter case more closely resembled the initial condition used in the numerical computations. With either scenario, flow began as soon as the heater was energized. Both scenarios produced the same quasi-steady flow pattern, but in the latter case this flow pattern developed sooner.

In the two-phase tests, one micron aluminum oxide particles were stirred into the liquid prior to heating, and again the liquid motion decayed prior to the initiation of heating. An oil-based smoke tracer was applied in liquid form to the heater surface to visualize the vapor phase flow in these tests. As the heater was energized, the liquid coating vaporized/pyrolized and eventually smoked, providing a simple and relatively quiescent injection method to trace the flow. When smoke fell onto the liquid pool surface, it served as a surfactant which reduced the thermocapillary-induced flow in the liquid phase. This technique was only used when it was desired to remove or reduce thermocapillarity from the problem and a non-vaporizing liquid was employed (with vaporization, smoke sometimes served as condensation nuclei and recondensed vapor which had evaporated from the liquid pool surface).

Results: Single-Phase Tests, Normal Gravity

The experimentally observed flow patterns depended on heater temperature. When this temperature was below 650 K (note that this is the centerline steady-state temperature), only one large toroidal cell formed in the container. Between 650 K and 750 K, only a single cell was distinguishable initially, as shown in Figure 4. Eventually the single cell formed a "figure-8"-pattern (faintly visible in Figure 5), with the second vortex being much weaker than the upper cell. For heater temperatures between 750 K and 820 K (the maximum temperature investigated), two toroidal cells separated by a saddle point appeared inside a large "figure-8"-cell (see Figure 6).

These results were obtained with a 1.2 cm diameter heater. Additional tests with a larger diameter heater (2.5 cm) produced similar vortices, but the "figure-8" formation first occurred at lower temperatures. In both systems, after 5 to 10 minutes, the axisymmetry of the observed flow patterns often broke down—for unknown reasons—and the tests were terminated.

In most tests increasing the heater temperature decreased the height of the upper vortex as a result of the "figure-8" formation; however in some tests only a single cell remained, even at large times. The height of the cell was larger (extended much lower toward the bottom of the container) than for tests made at a lower heater temperature. This anamolous behavior may have been due to plateout of the tars of the tobacco smoke on the container and the heater which affected the radiation heat transfer over the course of several experiments. We would expect that as the Grashof number increases (e.g., by increasing the heater temperature) or as the radiation heat transfer increases for a given Grashof number, the number of recirculation cells should increase.

To test this explanation, simulations were run without including the effect of radiation. For simplicity, an isothermal heater (682 K) was used. The result was that, similar to some experiments, one large toroidal cell formed in the container, the strength of which changed very little from $t = 5$ seconds to $t = 100$ seconds. A comparison of the nondimensional stream function contours with and without radiation for $t = 100$ seconds appears on Figure 7. Note that the left side of the computational domain corresponds to the axis of symmetry of the test cell. The nondimensional stream function, ψ, is defined by

$$\psi = -\int_0^r \rho r v dr, \qquad \psi = r\int_0^y \rho u dy$$

where

$$\psi = \psi'/\psi_*, \quad \psi_* = (\rho U L)_* = 5.915 \text{ x } 10^{-4} \text{ kg/(m·s)}$$

The maximum value of the stream function for the single vortex without radiation is only 8% less than the local maximum value of the upper vortex for the case including radiation. However, the flow pattern is qualitatively very different since only one large cell is formed instead of three. Thus the qualitative flow pattern is a strong function of the radiative heat transfer.

The difference between the flow patterns of Figure 6 and 7a is due to the radial distribution of the heater temperature. When a radially-varied heater temperature profile was simulated, as occurs in the experiments, a "figure-8"-shaped flow pattern resulted with a saddle point separating two clockwise-rotating vortices. Figure 8 shows a comparison with an isothermal (792 K) heater after $t = 60$ seconds in terms of the nondimensional stream function (note that negative values of the stream function correspond to clockwise rotation). As shown on Figure 8, when a constant-temperature heater profile was used three separate recirculation cells formed in the flow field. The middle vortex is relatively small in size and is also weaker in strength than both the upper and lower vortices. The flow pattern of Figure 8b is qualitatively similar to that observed experimentally (see Figure 6). The difference in the flow patterns between the constant versus radially-varying heater temperature

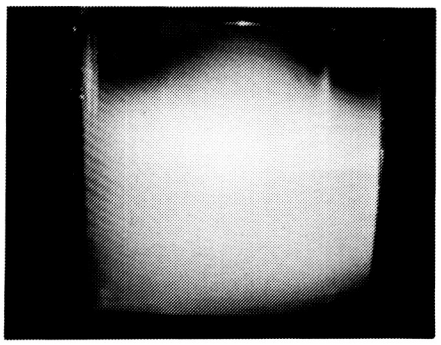

(a) $t = 4$ seconds

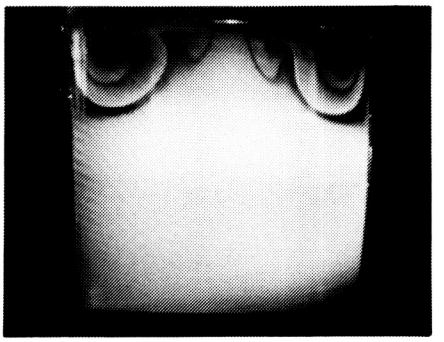

(b) $t = 15$ seconds

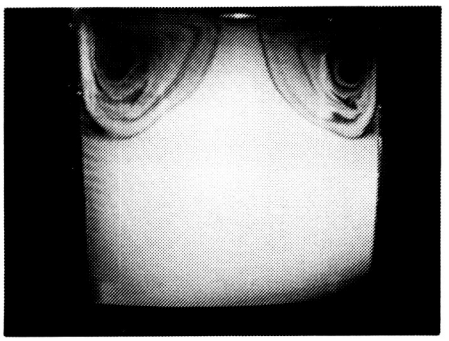

(c) $t = 30$ seconds

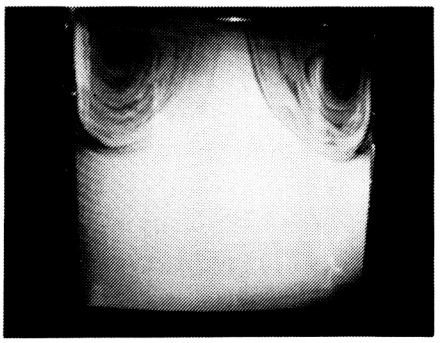

(d) $t = 50$ seconds

Figure 4: Flow patterns obtained in experiments using 682 K heater for (a) $t = 4$, (b) $t = 15$, (c) $t = 30$, and (d) $t = 50$ seconds. Only one toroidal-shaped vortex is distinguishable. Smoke tracers and low-power laser light sheet were used for flow visualization.

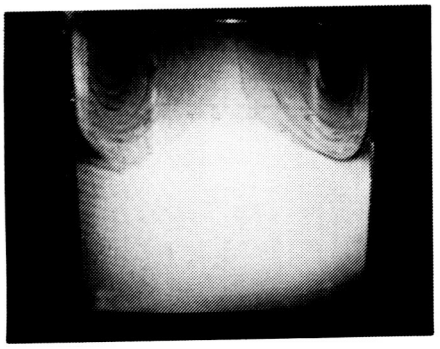

(a) $t = 60$ seconds

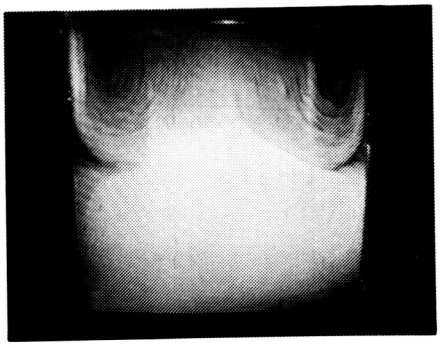

(b) $t = 80$ seconds

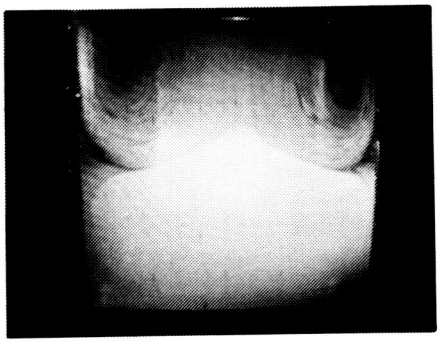

(c) $t = 100$ seconds

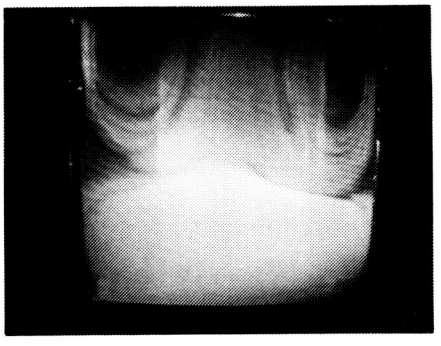

(d) $t = 200$ seconds

Figure 5: Flow patterns obtained in experiments using 682 K heater for (a) $t = 60$, (b) $t = 80$, (c) $t = 100$, and (d) $t = 200$ seconds. Outline of relatively weak lower vortex is faintly distinguishable.

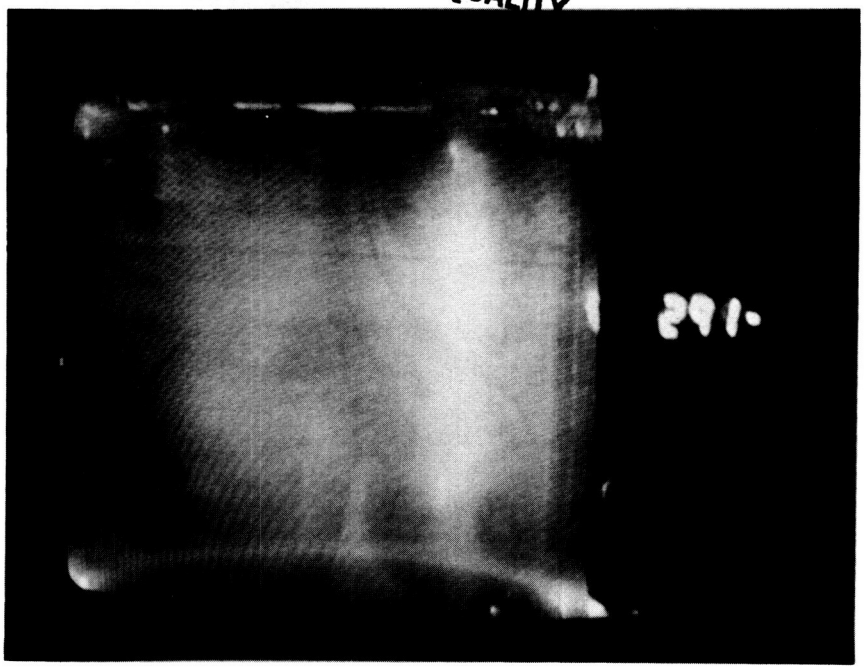

Figure 6: Flow pattern observed for a 790 K heater (t = 291 seconds).

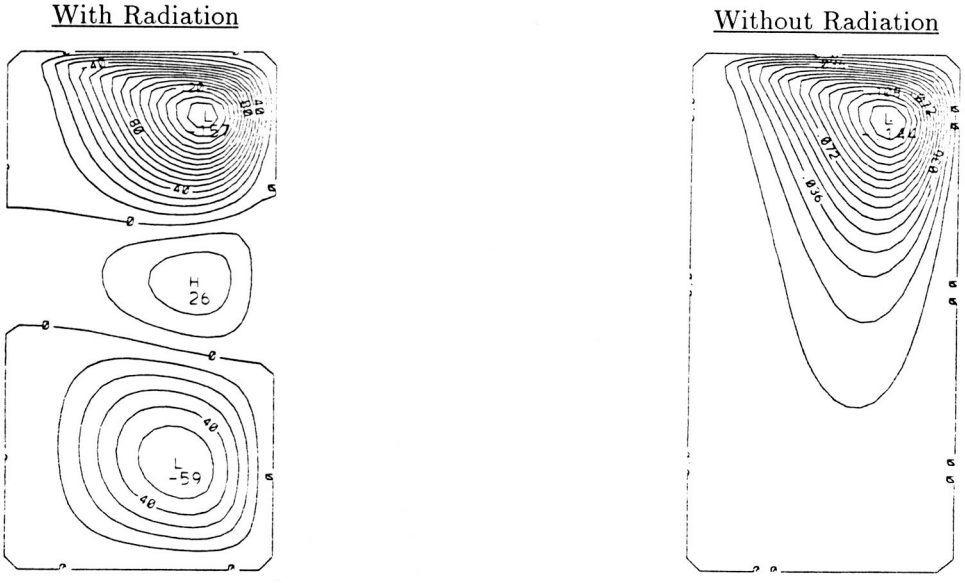

Figure 7: Comparison of the nondimensional stream function (ψ) contours with and without radiation for t = 100 seconds; $\psi_* = (\rho U L)_* = 5.915$ x 10^{-4} kg/(m·s). The heater was assumed isothermal at 682 K.

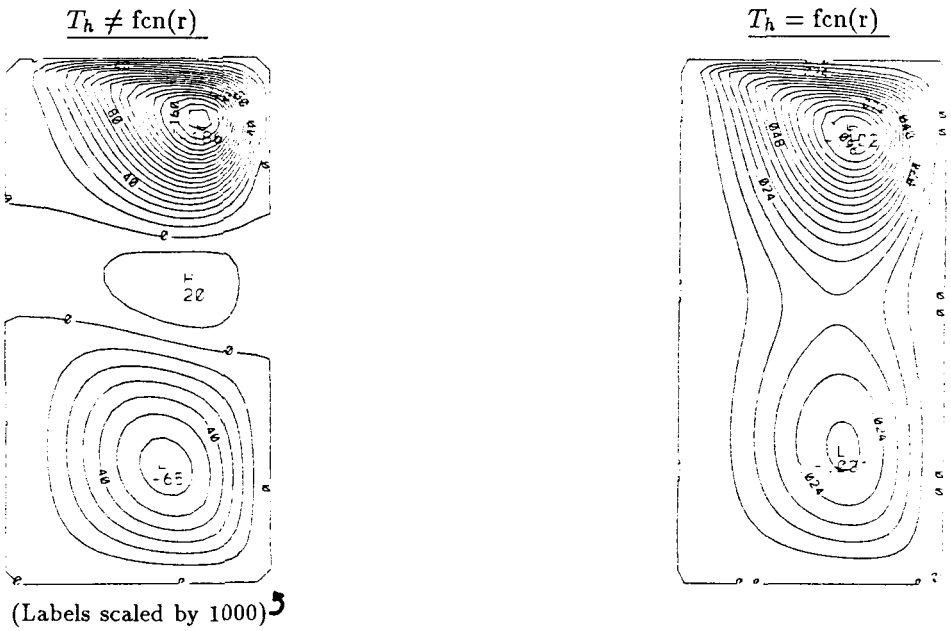

Figure 8: Comparison of the nondimensional stream function (ψ) contours at $t = 60$ seconds for constant versus radially-varying heater temperature profiles. The centerline heater temperature was 792 K for both cases.

profiles is due to the difference in the buoyancy effect of the heater. An additional effect of a change in the heater temperature profile is a change in the radiative heat flux to the container walls which may act as secondary heat sources to the flow. However, the difference in radiative heating of the walls is not great enough to change the flow field from the "figure-8"-shaped flow pattern to the three separate recirculation cells. This is because the area-weighted average temperature of the heater is approximately 550K versus 792 K for the radially-varying versus constant heater temperature profiles, whereas the side wall temperature after 60 seconds of the simulation is only approximately 300.2–300.3 K for these two cases. Based on the comparison shown on Figure 8, one may conclude that the predicted flow pattern depends strongly on the actual radial heater temperature distribution.

Results: Two-Phase Tests, No Vaporization, Low Thermocapillarity

A few tests were run with the container partially filled with silicon oil. Under the test conditions, the silicon oil would have negligible evaporation. The oil-based smoke was used to visualize gas phase motion. The smoke apparently contaminated the liquid surface, reducing the thermocapillary-induced motion. Little liquid phase motion was observed, suggesting that liquid phase buoyancy is a weak force compared to the thermocapillary force. In the gas phase, a large toroidal cell was observed, as shown on Figure 9, when the heater was operated at about 800 K. Note that this flow pattern is substantially different than that observed in the single-phase tests at the same temperature but different aspect ratio. It should also be noted that if there was any significant liquid motion due to liquid phase buoyancy, then a small, recirculating gas phase cell should have been observed close to the liquid surface due to no-slip considerations. However, no such motion was observed.

The experimental results shown on Figure 9 agree very well with the predictions of the numerical model. A 60-second simulation was made with a 1 cm diameter 800 K heater in a 10 cm diameter and height plexiglass container filled 5 cm with liquid n-decane. Vaporization and surface tension were not included in the simulation, although radiation was included. The resulting flow pattern in the gas phase predicted by the numerical model appears on Figure 10. Only one large toroidal-shaped recirculation cell appeared in the gas phase when surface tension was not included in the simulation. Although a different liquid was used, the Grashof numbers were similar for n-decane and silicon oil. The maximum velocity in the liquid phase was found to be only 0.04 mm/s (virtually no liquid phase motion). These findings are in agreement with the aforementioned experimental results.

Results: Single-Phase Tests, Reduced Gravity

Two types of single-phase phase simulations were made for a reduced gravity level of 10^{-5} g. In the first case, the gravity level begins at 10^{-5} g and remains at this level throughout the simulation. In the second case a simulation is first run for 100 seconds under normal gravity, after which the gravity level is abruptly changed to 10^{-5} g in order to simulate a drop tower experiment. For both

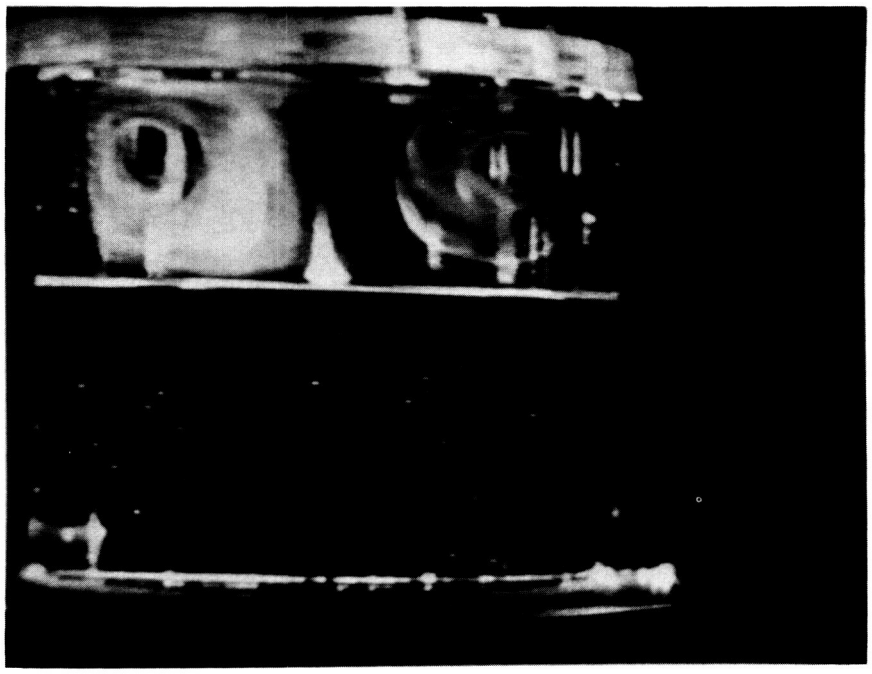

Figure 9: Two-phase test results with negligible vaporization and surface tension; the heater temperature is 800 K.

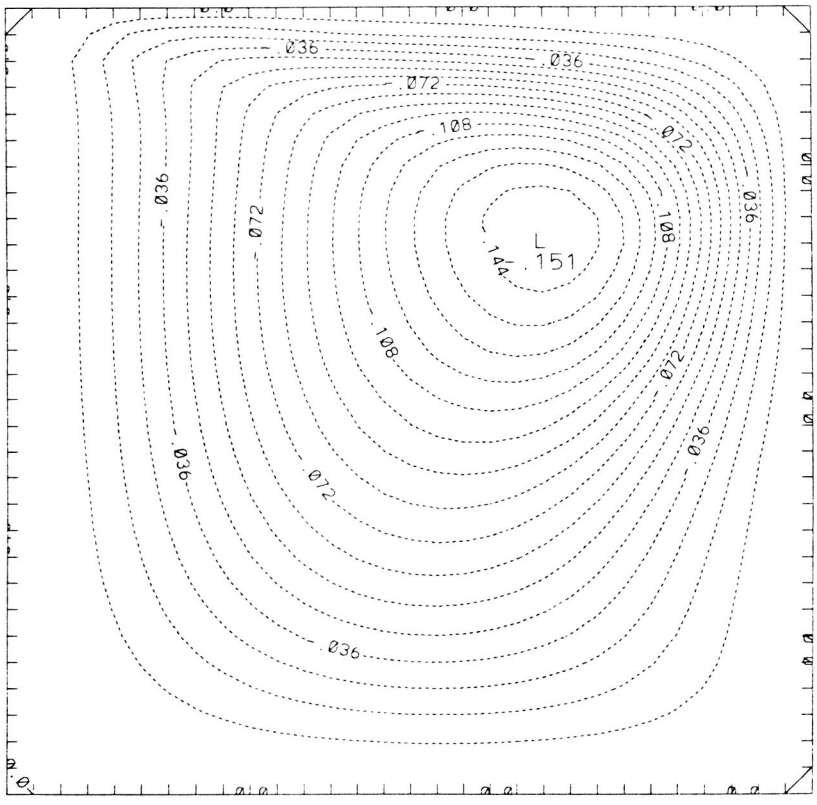

Figure 10: Gas phase nondimensional stream function (ψ) contours from two-phase (air and liquid n-decane) computer simulation with negligible vaporization and surface tension (t = 60 seconds); the heater temperature is 800 K.

simulations a 686 K (775°F) 1.2 cm diameter heater was used in a 10 cm (height and diameter) plexiglass container. The wall thickness of the container was taken to be 4 mm top and sides with a 12 mm bottom wall. In the first simulation, one recirculation cell formed and remained relatively unchanged after 20 seconds. The center of this recirculation cell was slightly left and above the center of the calculation domain. Its local maximum of the stream function was three orders of magnitude less than the value of the upper vortex in the normal gravity simulation.

In the drop tower experiment simulation, the flow field was first simulated for 100 seconds of normal gravity. During this time the flow reached a quasi-steady state. When the gravity level was then changed to 10^{-5} g, rapid changes occurred in the velocity and distribution of the velocity field over the first 2.2 seconds. In 2.2 seconds the maximum speed in the gas changed from 3.0 cm/s at r=0.4 cm and 0.25 cm below the top wall to 0.4 cm/s at r=0 and y=5.25 cm (4.75 cm below the top wall). The velocity at r=0.4 cm and 0.25 cm below the top wall was reduced to approximately 0.01 cm/s after 2.2 seconds. A plot of velocity vectors shows a significant change in the velocity distribution in the flow (with respect to the maximum speed). The implication of these results is that verification experiments can be made with distinguishable results in the 2.2-second drop tower. It is anticipated that results of such tests will be included at the time of the presentation. However, these tests were not completed in time for inclusion in this preprint.

Conclusions

A model has been developed for the transient response of an enclosed, two-phase system heated nonuniformly from above. Results of normal gravity experiments and simulations show qualitatively the same flow patterns.

The radiant heat transfer and the radial heater temperature profile are critical factors which influence the resulting flow pattern. The simulated results may deviate from the actual experiments because of the black-body radiation and step-change heater profile assumptions made in the computational model. These assumptions may be relaxed and hence a more accurate prediction of the flow may be made if surface emissivity and heater temperature profile data are collected.

Experimental results showed that a transition between one recirculation cell to a two-cell configuration separated by a saddle point occurs for heater temperatures between 750 K and 820 K for the single-phase system. In the future, different heater sizes and temperatures as well as various container sizes will be used in order to correlate these transitions to important parameters in the flow such as the Grashof number.

Drop tower experiments and simulations may be used to compare reduced gravity flow pattern results over a relatively short period of time (2.2 seconds) because the flow field responds quickly and dramatically to the near-step change in the gravity level. The most marked change in velocity occurs immediately below the heater where the velocity decreases by two orders of magnitude in 2.2 seconds.

Acknowledgement

Research at U.C.I. was conducted in support of NASA Grant No. NAG 3-627. The authors would like to thank Dr. H. Kim and Mr. T. Heist for assisting in the experimental data collection.

References

[1] Furuta, M., Humphrey, J. A. C., and Fernandez-Pello, A. C., "Prediction of Flame Spread Hydrodynamics Over Liquid Fuel," *Physico-Chemical Hydrodynamics*, Vol. 6, No. 4, 1985, pp. 347–372.

[2] Glassman, I. and Dryer, F. L., "Flame Spread Across Liquid Fuels," *Fire Safety Journal*, Vol. 3, 1980/1981, pp. 123–138.

[3] Sirignano, W. A. and Glassman, I., "Flame Spreading Above Liquid Fuels: Surface-Tension-Driven Flows," *Comb. Sci. Tech.*, Vol. 1, 1970, pp. 307–312.

[4] Murad, R. J., Lamendola, J., Isoda, H., and Summerfield, M., "A Study of Some Factors Influencing the Ignition of a Liquid Fuel Pool," *Combustion and Flame*, Vol. 15, 1970, pp. 289–298.

[5] Aggarwal, S. K., Iyengar, J., and Sirignano, W. A., "Enclosed Gas and Liquid with Nonuniform Heating from Above," *Int. J. Heat Mass Transfer*, Vol. 29, 1986, pp. 1593–1604.

[6] Abramzon, B., Edwards, D. K., and Sirignano, W. A., "Transient, Stratified, Enclosed Gas and Liquid Behavior with Concentrated Heating from Above," *J. Thermophysics*, Vol. 1, No. 4, October 1987, pp. 355–364.

[7] Altenkirch, R. and Vedha-Nayagam, M., Paper 3-D2, 1986 Spring Technical Meeting, Central States Section; The Combustion Institute.

[8] Patankar, S. V., Numerical Heat Transfer and Fluid Flow. Hemisphere and McGraw-Hill, New York (1980).

[9] Van Doormaal, J. P. and Raithby, G. D., "Enhancements of the SIMPLE Method for Predicting Incompressible Fluid Flows," *Numerical Heat Transfer*, Vol. 7, 1984, pp. 147–163.

NASA
National Aeronautics and Space Administration

Report Documentation Page

1. Report No.	2. Government Accession No.	3. Recipient's Catalog No.
NASA TM-101471 AIAA-89-0070		

4. Title and Subtitle

Behavior in Normal and Reduced Gravity of an Enclosed Liquid/Gas System With Nonuniform Heating From Above

5. Report Date

6. Performing Organization Code

7. Author(s)

H.D. Ross, D.N. Schiller, P. Disimile, and W.A. Sirignano

8. Performing Organization Report No.

E-4585

10. Work Unit No.

674-22-05

9. Performing Organization Name and Address

National Aeronautics and Space Administration
Lewis Research Center
Cleveland, Ohio 44135-3191

11. Contract or Grant No.

13. Type of Report and Period Covered

Technical Memorandum

12. Sponsoring Agency Name and Address

National Aeronautics and Space Administration
Washington, D.C. 20546-0001

14. Sponsoring Agency Code

15. Supplementary Notes

Prepared for the 27th Aerospace Sciences Meeting sponsored by the American Institute of Aeronautics and Astronautics, Reno, Nevada, January 9-12, 1989. H.D. Ross, NASA Lewis Research Center; D.N. Schiller and W.A. Sirignano, University of California at Irvine, Irvine, California 92664; P. Disimile, University of Cincinnati, Cincinnati, Ohio 45221.

16. Abstract

The temperature and velocity fields have been investigated for a single-phase gas system and a two-layer gas-and-liquid system enclosed in a circular cylinder being heated suddenly and nonuniformly from above. The transient response of the gas, liquid, and container walls was modelled numerically in normal and reduced gravity (10^{-5}g). Verification of the model was accomplished via flow visualization experiments in 10 cm high by 10 cm diameter plexiglass cylinders.

17. Key Words (Suggested by Author(s))	18. Distribution Statement
Natural convection Microgravity fluid flow Pool fires Thermocapillarity	Unclassified – Unlimited Subject Category 29

19. Security Classif. (of this report)	20. Security Classif. (of this page)	21. No of pages	22. Price*
Unclassified	Unclassified	12	A03

NASA FORM 1626 OCT 86

*For sale by the National Technical Information Service, Springfield, Virginia 22161